A Power Management Strategy for Multiple Unit Railroad Vehicles

Shaofeng Lu, *Student Member, IEEE,* Stuart Hillmansen, and Clive Roberts,

***Abstract*—Improved fuel consumption and lower emissions are two of the key objectives for future transportation. Hybrid Electric Vehicles (HEVs), in which two or more power systems are combined, are able to meet these objectives through the capture and reuse of regenerated braking energy, and through optimised use of the prime mover. However, more complicated power management strategies are required for such vehicles. This paper explores the potential of applying to advanced power management strategies for a Diesel Multiple Unit (DMU) train. These types of vehicles have multiple diesel engines which are commonly operated in a homogenous manner. The work presented in this paper analyses the potential energy savings that may be obtained through the independent operation of the engines. Two widely investigated power management strategies that have been developed for HEVs have been applied to a typical DMU railroad vehicle.**

Dynamic Programming (DP) strategies have been applied to the results produced by a Single Train Motion Simulator (STMS) to identify the optimal instant power distribution between the engines. An adaptive rule-based online strategy based on the optimization results from the DP solution is then proposed and realized using a non-linear programming optimization algorithm. Both of these two strategies indicate acceptable agreement and show around 7% fuel cost reduction in comparison with the evenly-split engine operation.

***Index Terms*—Energy management strategy, Multiple unit train, Dynamic programming, Rule-based online strategy, Non-linear optimisation**

I. Introduction

With the increasing concerns for the environment and fuel cost, railroad transportation is facing pressure to improve the environmental performance of its vehicles. To improve fuel economy and reduce total emissions, the propulsion systems are becoming more complex. As a result, multiple power sources are commonly present in modern railroad vehicles, as opposed to locomotive hauled trains. Two of notable examples of railroad vehicles which employ multiple power sources include prototype Hybrid Electric Vehicles (HEVs) (currently in the early stages of development), and more common Multiple Unit Vehicles. This introduction will briefly review recent research concerning HEVs with various power management strategies, and will then discuss a typical British Diesel Multiple Unit (DMU) train and its potential to employ advanced power management strategies.

Corresponding author S Hillmansen. School of Electronic, Electrical and Computer Engineering, University of Birmingham, Edgbaston, Birmingham, UK, B15 2TT e-mail: (s.hillmansen@bham.ac.uk).

Manuscript received May 19, 2009; revised January 11, 2010.

A. Power Management Strategies for Hybrid Electric Vehicles

The idea of hybridization of a propulsion system was originally conceived from the motivation to extend the working range of electric automobiles [1]. However, there are numerous additional benefits of these systems. A hybridized design with both prime mover (Internal Combustion Engine (ICE) or Fuel Cell) and on-board energy storage device, are often able to utilize a significantly down-sized prime-mover. The Energy Storage Device can enable the prime mover to operate within its optimum efficiency range and also capture braking energy [2], [3]. There is a large body of research which has focused on elevating the efficiency of components, such as power electronics devices [4], [5] and batteries [6]–[9].

In order to take full advantage of hybridization, effective power management strategies are necessary. Four key goals of a hybrid system are summarized below:

- maximum fuel economy;
- minimum emissions;
- minimum system costs;
- good driving performance.

The power management strategy needs to consider: the optimal engine operating region, engine dynamics, minimum engine speed, battery state of charge, relative power distribution, *etc* [10]. These strategies can be primarily divided into two categories: rule-based and optimization-based [11].

A rule-based strategy consists of sets of if-then rules in an expert system. These sets of if-then rules can be obtained from heuristics, human experience or simulation results. Rule-based strategy attributes its notable advantages to having no requirement for the future journey profile to be known, and is also suitable for on-line applications. The main idea behind a rule-based strategy for HEVs is "Load leveling". Load leveling suggests that one operates the ICE in its optimal region. The difference between the output of the ICE and the demands of the driver will be met by the energy storage device [12]. Recent work has shown that the Equivalent Consumption Minimization Strategy (ECMS) can be used to determine an effective rule-based strategy to achieve a fuel saving [13]. Within the scope of rule-based strategies, fuzzy rule-based strategies [14]–[16] as a robust control method, is suitable for highly non-linear, multi-domain, time-varying systems such as HEV propulsion systems.

Several optimization-based control strategies for power management of HEVs have already been proposed. These control strategies could generally be categorized into two groups: global off-line optimization and on-line optimization [17], [18].

TABLE I
TYPICAL TECHNICAL DATA FOR DMU TYPE VEHICLES

Technical Data	
Track gauge	$1435mm$
Number of cars per unit	2 to 6 cars; basic version 3-car unit
Unit length	standard
Max. operational speed	160 km/h
Power supply	1 Diesel motor (560 kW) in each car
Unladen weight	approx. 168.5 tonnes
Maximum axle load	18.5 tonnes

Global optimization methods are rarely suitable for on-line implementation. However, these solution methods can give useful information for designing on-line strategies. Dynamic Programming [19] [20], Non-Linear Convex Programming [21], Genetic Algorithms [22], [23], and Optimal Control Theory [24] [25] have all been applied to develop the power management strategy of HEVs.

B. Typical DMU train

The traditional traction system of a DMU train consists of several homogeneous power sources. Multiple unit trains usually operate the individual engines in a synchronized manner. This means that engines can often operate well outside their optimum operating region. For example, a set of engines may all work with a low power output resulting in an inefficient operation. The central hypothesis of the current paper is that by decoupling the engines and operating them individually, the overall efficiency can be improved. This paper will take a typical DMU train as a case study and demonstrate the application of advanced power management strategies. Dynamic Programming (DP) will be used to develop the off-line global optimization strategy, and the results will then be used to develop the on-line rule-based strategy.

Fig. 1(a) shows a schematic of the traction system arrangement of a DMU train. A diesel engine with maximum output power of 560 kW is installed in each car. The sizing of the engines used in this work has been closely based on realistic vehicles, for example the BR class 185 [26]. Fig. 1(b) is a simplified overview of the drive system. Table I presents some technical data for this type of vehicle.

An "Eco-Mode" programme has actually been initiated in-service for the class 185 to maximize the energy efficiency. The Eco-Mode Phase 1 yielded significant savings, and in the next phase of the work the fuel economy is expected to further improve. The core concept of Eco-Mode is the selective use of the 3 engines [27]. The work presented in the current paper is inspired by the "selective operation" concept and investigates more deeply from a mathematical and optimization viewpoint. The technique discussed in the current paper uses global optimization, theoretically leading to improved fuel economy and optimal operation of the three engines.

II. METHODOLOGY

To support the study of the traction system optimization, a Single Train Motion Simulator (STMS) has been developed to simulate the power requirements of a train undertaking a typical journey. Since the main purpose of the optimization is to minimize the fuel consumption of the engines, the engine characteristic is also an important input into the analysis. This section will cover both the STMS and engine characteristic in parts II-A and II-B respectively.

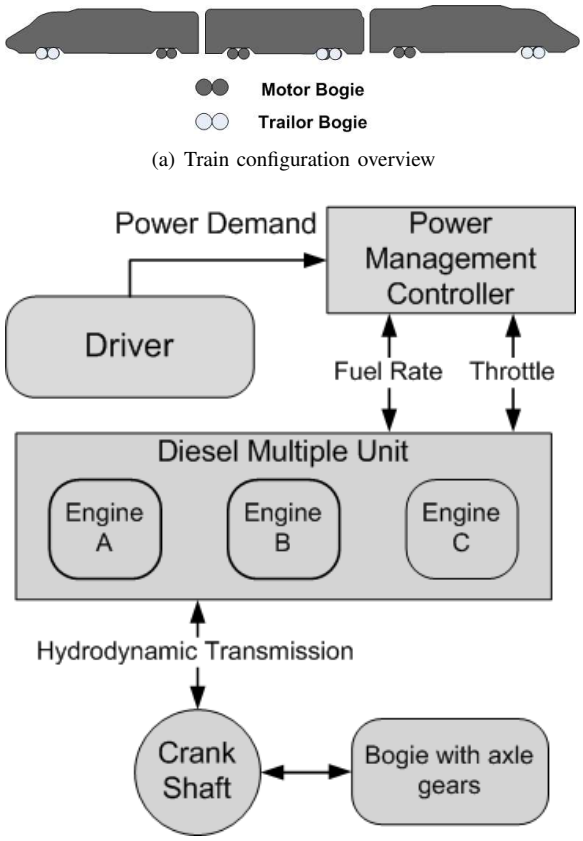

(a) Train configuration overview

(b) Train drive system overview

Fig. 1. A typical 3 coach DMU train

A. Vehicle Modeling and Simulation

1) Equations of motion: The motion of the single railroad vehicle is generally deterministic regardless of random disturbance from outside environment [28]. The required duty cycle is dependent on different factors of the train operation. For instance, the detailed profile of gradients, speed limit, train mass and passenger loads *etc.* is necessary information in order to calculate the motion of the train.

In a typical single train duty cycle between two stations, at low speed the adhesion limit defined by (1) sets the maximum available tractive effort (F).

$$F = \mu M g \tag{1}$$

At higher speed the power becomes the main limiting factor. In Fig. 2, the vehicle keeps a constant tractive effort up to a particular point referred to as the "base speed" and then has a constant power region which has the effect of decreasing the tractive effort reciprocally. Acceleration is maintained up to the balancing speed where the installed tractive capacity is equal to the combined resistance and gradient forces.

Energy for the railroad traction system is used for acceleration, overcoming electrical and mechanical power losses

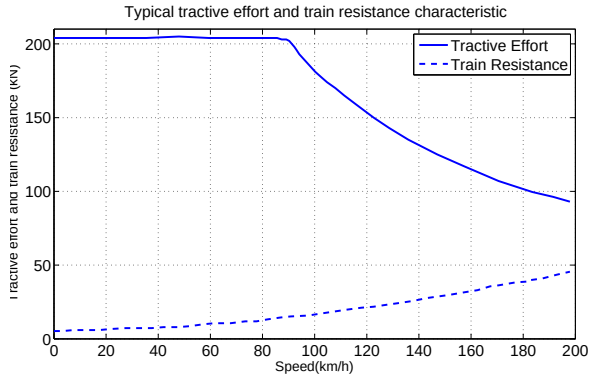

Fig. 2. Typical railroad vehicle tractive effort and resistance characteristic

and for work in moving the mass of train forward against the frictional forces.

The basic equation of motion is based on Newton's Second Law:

$$M^* \frac{\mathrm{d}^2 s}{\mathrm{dt}^2} = F - R - Mg\sin(\alpha) \tag{2}$$

where:

- M^* is the effective vehicle mass (including rotational inertia);
- M is the vehicle mass;
- g is the acceleration due to gravity;
- R is the vehicle resistance to motion;
- F is the tractive effort;
- s is the vehicle position.

Consideration of the following issues is important in order to solve (2).

1) **Adhesion** The frictional force between the driven steel wheels and rail is the actual tractive force which moves the train forward. The value of the adhesion force on one driven axle can be calculated using (1), where μ is the coefficient of friction. In railroad applications, this value ranges from 0.05 to 0.5 depending on the conditions. The upper limit of 0.5 is sometimes assumed when encountering dry or sanded track. The maximum tractive effort (TE_{max}) per axle is therefore limited by:

$$TE_{max} < \mu Mg \tag{3}$$

In order to maximize the total tractive force, it is usual to increase the proportion of motored axles. The maximum acceleration on flat track can be expressed by:

$$\frac{\mathrm{d}^2 s}{\mathrm{dt}^2} = gp\mu \tag{4}$$

where:

- g is the acceleration due to gravity ;
- p is the proportion of motored axles;
- μ is the coefficient of friction.

The coefficient of friction is assumed to be independent of the speed of the train, but in reality there is some decrease at high vehicle velocities.

2) **Resistance** The motion of train is opposed by a number of resistive forces. The overall resistance on level track can be formulated as follows:

$$\begin{aligned} R &= (A' + B'v)M + Cv^2 + \frac{D}{r} \\ &= A'M + B'Mv + Cv^2 + \frac{D}{r} \end{aligned} \tag{5}$$

Where A', B', C and D are empirical constants, M is vehicle mass, v is the velocity and r is the radius of track curvature. The constant terms in (5) are commonly obtained using empirical methods [29]. (6) is a simplified version that is used in the current work. In this equation, the constants include the effect of mass, and the increase in resistance due to track curvature has been assumed to be negligible.

$$R = A + Bv + Cv^2 \tag{6}$$

Where v is the velocity (m/s) and the coefficients A(kN), B(kNs/m) and C(kNs^2/m^2) characterize the resistance to motion.

3) **Effective Mass** The rotational inertia of the rotating components on the train must be taken into account in order to properly calculate the acceleration of the train. This is usually done by adding a rotary allowance term to the mass of the train. This is expressed as a fraction of the tare mass of the train.

$$M^* = M(1 + \lambda_w) + M_l \tag{7}$$

Where:

- M^* is the effective mass;
- M is the tare mass;
- λ_w is the rotary allowance;
- M_l is the freight or passenger load.

Alternatively, for the sake of simplicity, the effective mass could be simply expressed by:

$$M^* = M \times (1 + \lambda_w) \tag{8}$$

The rotary allowance λ_w is a constant (usually less than 0.2) and depends on the proportion of motored axles, the gear ratio and type of vehicle construction.

The general equation of train motion, known as as Lomonossoff's equation, can be written as follows:

$$M^* \frac{\mathrm{d}^2 s}{\mathrm{dt}^2} = F - (A + B\frac{\mathrm{d}s}{\mathrm{dt}} + C\frac{\mathrm{d}s}{\mathrm{dt}}^2) - Mg\sin(\alpha) \tag{9}$$

Here F is the tractive effort and A, B, and C are constants from the Davis Equation (6).

2) Single train motion simulator: A Single Train Motion Simulator (STMS) has been developed using Lomonossoff's equation. An overview schematic is shown in Fig. 3. In Fig. 3, four parts of the simulator are shown. From left to the right, they are:

1) Driving style instructor. This block acts like an train driver, giving instructions to the train traction system. For example, there are two driving styles which are easy to identify: driving the train as fast as possible and driving the train as energy efficient as possible within

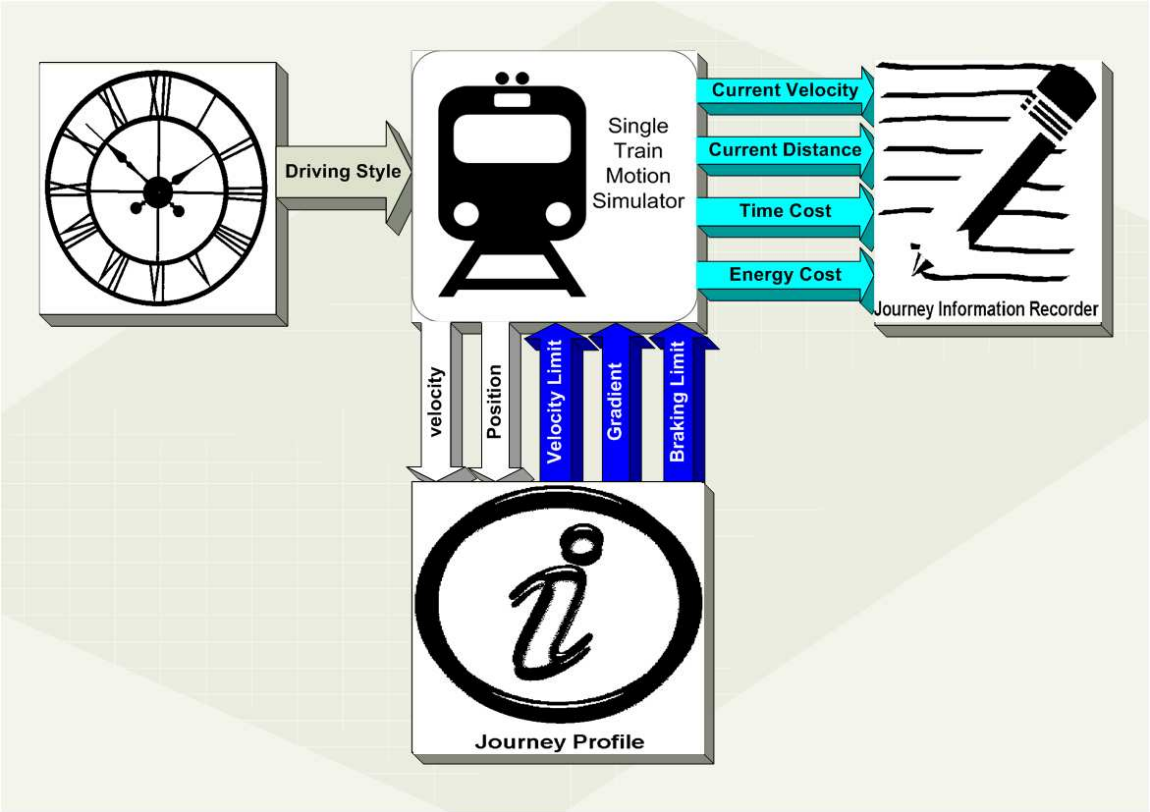

Fig. 3. System diagram of single train simulator diagram

acceptable journey times. Since this study focuses on the engine power distribution, the driving style is selected to be "As fast as Possible", i.e., "flat out running".

2) Journey Profile. The journey profile, including the signaling system, geographic information, velocity limit and station position, are all determined for a known journey. In this study, journey profiles are stored in a look-up table which is loaded before the simulation. The STMS calculates the velocity and acceleration of the train as it moves through the simulated journey by solving Lomonossoff's equation using one computational second time step.
3) Journey Information Recorder. To demonstrate the simulation results, the output results are stored in the Journey Information Recorder. At each time step, the position of the train, the velocity of the train, and the energy consumed are recorded.
4) Single Train Motion Simulator. This block is the Central Processor Unit for the whole Simulator.

There are 5 operation modes for the traction system that are available to the train.

1) Constant Tractive Effort Mode. The train is accelerated under a constant tractive effort. This mode is invoked at the beginning of the journey.
2) Reduced Power Mode. The train is accelerated under a reduced power condition. This mode is active when the train is approaching the velocity limit or braking limit curve to reduce the acceleration.
3) Constant Power Mode. Above the base velocity of the train, the constant Tractive Effort Mode switches to a Constant Power Mode to continue to accelerate the train.
4) Reducing Velocity Mode. If at anytime, should the velocity of the train overshoot the velocity limit, this mode will be turned on to quickly reduce the velocity.
5) Braking Power Mode. This mode is for the braking operation. The basic philosophy behind this can be interpreted by (10).

$$v_b = \sqrt{2aS} \tag{10}$$

Where:

- a is the braking deceleration imposed by constant braking effort;
- v_b is the proposed velocity for braking;
- S is the distance to the next station.

If v_b is greater than the current velocity, the braking mode should be activated, ensuring that the train is stopped completely at the next station.

For example, using the current velocity of the train, the processor is able to select whether the Constant Traction Mode or Constant Power Mode is active and then sets the state for the next calculation step. The Constant Traction Mode selects a constant traction effect for train operation, while in Constant Power Mode, the tractive effort is calculated using (11).

$$F = P_{max}/v \tag{11}$$

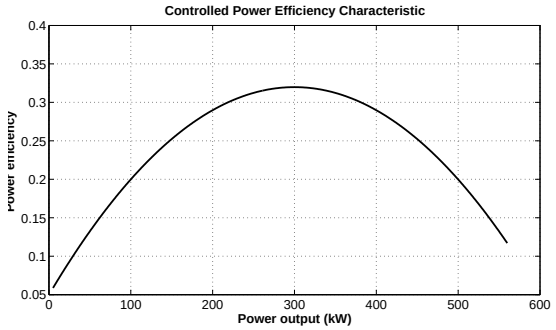

Fig. 4. Controlled diesel engine power efficiency characteristic

Where:

- F is the Tractive Effort;
- P_{max} means the current Maximum Engine Power;
- v is the current velocity of the train.

The parameters for the Single Train Simulator are shown in Table II.

B. Engine Description

1) Engine Efficiency Map: The diesel engine is represented by a nonlinear static efficiency map which describes the instantaneous Brake Specific Fuel Consumption (BSFC) of the engine with different engine speeds and engine output power.

$$\zeta = f(P_e, \omega) \tag{12}$$

$$\eta = \zeta / P_e \tag{13}$$

$$P_e = T\omega \tag{14}$$

Where, ζ is the fuel rate in gram per second (gs^{-1}), η is BSFC in gram per joule (gJ^{-1}), T is the engine output torque and ω is the engine speed. To simplify, engine power efficiency is defined by (15):

$$\eta = P_e / P_f \tag{15}$$

Where the P_f is the power converted from the fuel at a fuel rate of ζ.

The engine speed and power in this simulation has been limited to a single operating line on a typical engine efficiency map, i.e. each engine output power corresponds to a unique engine speed (following a propeller curve). The relationship between output power and fuel cost is convex, which is typical for most engines [21]. This convex shape implies that the most efficient operating point is below the maximum power output [30]. A characteristic fuel efficiency curve of a diesel engine used in similar simulation studies is displayed in Fig. 4 [31].

2) Energy Consumed Calculation: Each iteration step in the STMS is one second, thus the average power over that time step is numerically equivalent to energy consumed in that time step. The total energy consumption is calculated by integrating the power history. Between one iteration step and the next, there is a limitation for the power slew rate of each engine. It has been assumed that in II-B1, within one second, the Maximum Power Switch P_{mps} from one state to another is 30 kW. This means that the maximum total power difference from one second to the next is ± 90 kW.

III. Problem Definition

The optimization is inspired by the fact that the total power demand can be met by a combination of unique power outputs from each engine. Additionally, the individual engine states are constrained by previous engine states and restrict the future engine states (governed by the positive and negative engine power slew rates). This enables a complex decision making procedure to be defined in order to calculate the required output power from each engine.

The first part of this section will introduce the optimal objective and constraints. The second part will review the relationship between engine states and fuel cost.

A. Optimal objective and constraints

The objective of the power management strategy is to improve the fuel economy of the vehicle by distributing the power demand between the 3 engines. This can be formulated as an optimization problem:

$$\min_x J(x) \text{ subject to } G(x) \leq 0 \tag{16}$$

The cost function $J(x)$ represents the total fuel cost in an arbitrary duty cycle within a time length t_c (as expressed in (17)). $G(x) \leq 0$ accounts for the linear constraints.

$$J(P_{\mathrm{A}}, P_{\mathrm{B}}, P_{\mathrm{C}}) = \int_0^{\mathrm{t_c}} \mathrm{fuelrate}(P_{\mathrm{A}}, P_{\mathrm{B}}, P_{\mathrm{C}})\, dt \tag{17}$$

The operation limitations of each engine set the boundaries for each engine power $P_{\mathrm{A}}, P_{\mathrm{B}}, P_{\mathrm{C}}$. 18 illustrates that at any time during the journey, the engine can not exceed its operation limit defined by equations (19) and (20).

$$\begin{aligned} &P_{\mathrm{A\ min}}(t) \leq P_{\mathrm{A}}(t) \leq P_{\mathrm{A\ max}}(t) \\ &P_{\mathrm{B\ min}}(t) \leq P_{\mathrm{B}}(t) \leq P_{\mathrm{B\ max}}(t) \\ &P_{\mathrm{C\ min}}(t) \leq P_{\mathrm{C}}(t) \leq P_{\mathrm{C\ max}}(t) \qquad \forall t \in [0, t_{\mathrm{c}}] \end{aligned} \tag{18}$$

The upper limit $P_{\mathrm{e\ min}}$ and lower limit $P_{\mathrm{e\ max}}$ of each engine power output varies depending on the previous engine output $P_{\mathrm{e\ pre}}$, Maximum Power Switch (effectively the maximum power slew rate) P_{mps} and Maximum Power Output. The decision process can be expressed as follows:

$$P_{\mathrm{e\ min}} = \begin{cases} P_{\mathrm{e\ pre}} - P_{\mathrm{mps}} & \text{if } P_{\mathrm{e\ pre}} - P_{\mathrm{mps}} > 0 \\ 0 & \text{if } P_{\mathrm{e\ pre}} - P_{\mathrm{mps}} \leq 0 \end{cases} \tag{19}$$

$$P_{\mathrm{e\ max}} = \begin{cases} P_{\mathrm{e\ pre}} + P_{\mathrm{mps}} & \text{if } P_{\mathrm{e\ pre}} + P_{\mathrm{mps}} < P_{\mathrm{max}} \\ P_{\mathrm{max}} & \text{if } P_{\mathrm{e\ pre}} + P_{\mathrm{mps}} \geq P_{\mathrm{max}} \end{cases} \tag{20}$$

It is assumed at every instance that the driver's power demand P_d should be satisfied and the following condition should be met:

$$P_{\mathrm{d}}(t) = P_{\mathrm{A}}(t) + P_{\mathrm{B}}(t) + P_{\mathrm{C}}(t) \tag{21}$$

TABLE II
KEY PARAMETERS FOR SINGLE TRAIN MOTION SIMULATOR

Effective Mass(tonnes)	Maximum Power(kW)	Constant Torque(kN)	Approximate Braking Effort(kN)	Davis coefficients		
				A(kN)	B(kN/(m/s))	C(kN/(m/s)^2)
168.5	1680	66.12	-82.65	5.42	0.07	0.012

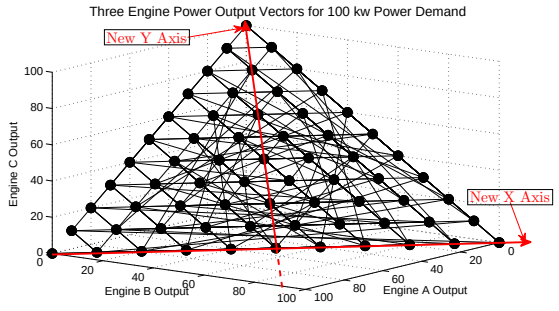

Fig. 5. Total power state vector in 3-D space. The magnitude of the vector is 100 on any point on the triangular surface

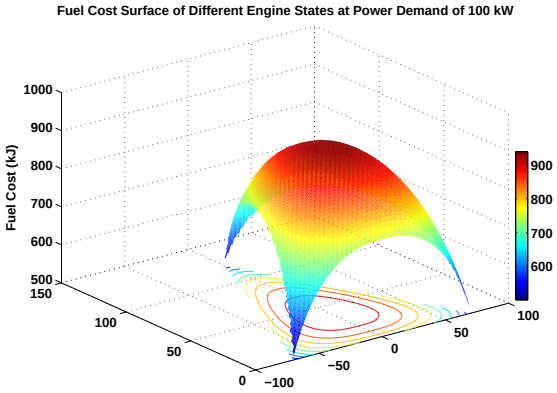

(a) Fuel cost map for power demand of 100kW

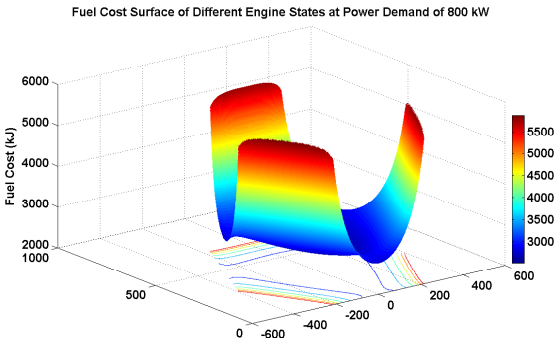

(b) Fuel cost map for power demand of 800kW

Fig. 6. Relationship between engine states and fuel cost under various power demand

B. Total Power State Vector and Fuel Cost

The total power state vector is represented by $[P_{\mathrm{A}}(t), P_{\mathrm{B}}(t), P_{\mathrm{C}}(t)]$. As has been stated in (21), all the engine output should meet the current power demand. If all the possible combination of engine outputs are plotted in 3-D space, a triangle plane is produced as shown in Fig. 5.

In Fig. 5, some of the engine states represented by black circles have been plotted on a triangular plane. At any point on this plane the magnitude of the total power state vector is constant. Since all the engine output must be non-negative, this triangular plane is only in the positive quadrant vector space, mathematically expressed as $Q = ((X, Y, Z)|X, Y, Z \geq 0) \in R^3$.

An axis transformation is performed to demonstrate the relationship between the engine states and the fuel cost. The new Y axis and X axis are shown in Fig. 5. The new Z axis is perpendicular to both the new X and Y axes and represents the fuel cost based on the data within the triangle. The transformation has the following features:

1) The higher the power demand is, the larger the area covered by the triangle.
2) The three vertices of the triangle each represent single engine operation.
3) The edges of the triangle represent dual engine operation.
4) Any point on the surface (not on an edge or vertex) represents triple engine operation.

After the axis transformation, by applying the fuel cost function described in section II-B, the relationship between different total power state vectors and fuel cost is demonstrated in Fig. 5 for both high and low total power demands.

In Fig. 6(a) and Fig. 6(b), it is easy to identify that a significant change occurs when power demand increases from 100 kW to 800 kW. When the power demand is 100 kW, the fuel cost is highest in the center area and lowest in the edge area. This implies the most fuel efficiency operation is to use one engine. At 800 kW, shape of the fuel cost surface is inverted and the most efficient operation is where all three engines are used equally.

Both of the two cases in Fig. 6 raise the possibility of complex dynamic decision making. Subject to the total power demand, the most efficient engine operation will change dynamically. The constraints of the power slew rate of each engine adds additional complexity. The solutions and results to this problem are discussed in section IV using two different methodologies.

IV. SOLUTIONS AND RESULTS

This section proposes two typical methodologies for fuel efficient power management strategies. Section IV-A will investigate the application of one global optimization strategy: Dynamic Programming (DP) based on Bellman's Principle of

Optimality [32]. Section IV-B will discuss an adaptive on-line power management strategy developed from DP. Due to the requirement for the whole journey profile to be known in advance, and the intensive CPU time associated with this method, DP is not suitable for on-line optimization. However, the results from DP can provide expert system rules information which can be incorporated into on-line applications [33].

A. Dynamic Programming

1) Introduction: Dynamic programming is a method for discrete optimization problems in which a set or sequence of decisions should be made in order to optimize the objective function. For each decision, the subproblem can be solved in a similar manner. An optimal solution of the original problem can be found from optimal solutions of every sub-problem [34].

The DP method is based on Bellman's Principle of Optimality: "An optimal policy has the property that whatever the initial state and the initial condition are, the remaining decisions must constitute an optimal policy with regards to the state resulting from the first decision " [32]. This assertion points out that the optimal policies could be derived from the suboptimal polices whose improvement will give rise to the improvement of the whole policy.

The optimization procedure using dynamic programming could have the mathematical form of $opt_{d\in\Delta}H(d)$,where:

- d is called the *decision*.
- Δ is the decision space where the *decisions* are chosen from.
- The optimand, H, is called the *Objective function*

In this case study, the *decision* is a series of engine state vectors. Δ represents the possible series of engine state vectors. For the optimum objective function, the expression is $H^* = H(d^*)$, where d^* is that value of $d \in \Delta$ for which $H(d)$ has the optimal results. d^* is the optimum decision for the engine states for the whole journey.

Instead of enumerating all the possible solutions concurrently in a "Brute Force" approach, the decisions are to be made in some specified sequence $d_1, d_2, d_3 \ldots, d_n$, so that:

$$\begin{aligned} H^* &= opt_{(d_1,d_2,d_3\ldots,d_n)\in D}\{h(d_1,d_2,d_3,\ldots,d_n)\} \\ &= opt_{d1\in D1}\{\ldots\{opt_{d_n\in D_n}\{h(d_1,d_2,d_3,\ldots,d_n)\}\}\ldots\} \end{aligned} \tag{22}$$

(22) is a **Sequential Decision Process**.

The basic form of a dynamic programming functional equation is:

$$f(S) = opt_{d\in D(S)}\{R(S,d)\circ f(T(S,d))\} \tag{23}$$

where:

- S is the engine state at each time step
- d is the engine power change at each pair of adjacent time steps.
- $R(S,d)$ fuel cost in the current engine state S.
- $f(T(S,d))$ is a next engine state transformation or transition function, assumed as zero cost for engine states transition.
- $\circ$ sums the fuel cost for a single decision.

An optimal decision consists of a series of engine state vectors, i.e.$[P_A(t), P_B(t), P_C(t)]$, where $P_A(t)$, $P_B(t)$ and $P_C(t)$ is the instant power output from engine A, B, and C respectively. The optimization problem now is changed into seeking an optimal decision in the decision space which could minimize the total fuel cost defined in (23).

2) Optimal Substructure: To illustrate this idea more explicitly, a diagram is shown in Fig. 7.

In Fig. 7, each circle symbolizes one possible engine state at that power demand. There are N power demand data and each power demand is denoted by P_i. Here i is the time sequence number of the power demand. $S_{i,j}$ denotes the engine state vector for the j_{th} engine state at power demand of P_i, where $j \leq M_i$ if there are M_i possible power state vectors for a power demand of P_i. Each engine has a fuel cost based on the fuel efficiency map in Fig. 4, denoted as $E_{i,j}$ for each power state vector $S_{i,j}$. The real line arrow represents the search directions and the dashed arrows are for the optimal path.

Generally, the number of possible power state vectors are innumerable. To simplify the search some assumptions have been made:

- There are two types of state vector which should always be included in the engine state vector searching space. One is an evenly operating mode vector in which power demand is evenly divided between all the engines, and the other one is the least engine operating mode vector in which the fewest possible number of engines are used to achieve the power demand.
- The engine power states are assumed to have quantized values (with an increment of 30 kW). This will reduce the number of possible power state vectors without compromising grade of global optimality.
- To avoid duplication of power state vectors, one assumes that power output from engine A is no less than B and power output from B is no less than C.
- It is assumed that, during the braking and stopping operation, the power demand is zero and all engine outputs are zero. As the searching route will definitely go through zero output states, i.e. the zero power states are one of the optimum states series, the optimization could be operated separately from zero power demand to next zero power demand in a smaller searching space exactly as shown in Fig. 7.

The optimization procedure is performed backwards. In Fig. 7, suppose that the minimum fuel cost from $S_{N-3,2}$ to final state S_N, is through $S_{N-2,6}$. Now it can be concluded that the fuel cost from states $S_{N-2,6}$ to final state S_N must also be minimum. The reason for this is that if there are other possible routes between $S_{N-2,6}$ and final state S_N which cost less fuel and are also reachable from $S_{N-3,2}$, we could easily substitute this path to yield a lower fuel cost from $S_{N-3,2}$ to the final state S_N. More generally speaking, for such engine states problems, an optimal solution to a problem (searching for minimum fuel cost through $S_{N-3,2}$ to the final cost), contains an optimal solution to the subproblem, i.e. obtaining

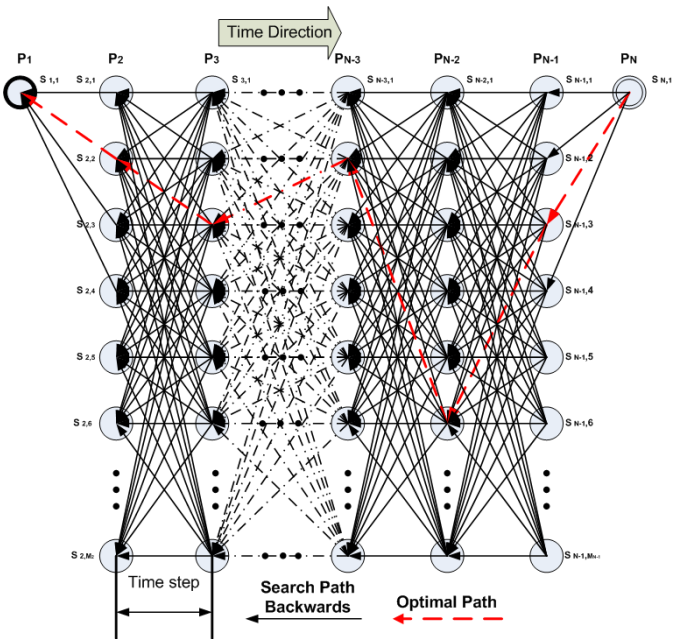

Fig. 7. Dynamic programming evolution diagram

the minimum fuel cost engine state vector series through $S_{N-2,6}$. This property is referred to as optimal substructure making Dynamic Programming a suitable method for such a problem [35].

3) Solution: Dynamic Programming aims to find an optimal solution recursively from the optimal solutions to subproblems as discussed in IV-A2. $F_i[j]$ denotes the minimum fuel cost engine path from engine states $S_{i,j}$ to the final engine state. If $F_i[j]$ finally defines the minimum fuel cost engine path from $S_{1,1}$ to final states $S_{N,1}$, the optimal engine states path is found, denoted as F^*. F^* is defined in (24):

$$F^* = min(E_{1,1} + F_2[1], E_{1,1} + F_2[2], \dots E_{1,1} + F_2[M_2]) \tag{24}$$

Where, $E_{1,1}$ is the energy consumption of the first Engine state. For the first step, from $S_{N,1}$ to $S_{N-1,j}$, $F_{N-1}[j]$ could be defined in (25):

$$\begin{aligned} F_{N-1}[1] &= E_{N,1} + E_{N-1,1} \\ F_{N-1}[2] &= E_{N,1} + E_{N-1,2} \\ &\dots \\ F_{N-1}[M_{N-1}] &= E_{N,1} + E_{N-1,M_{N-1}} \end{aligned} \tag{25}$$

Note that if $S_{N,1}$ is not reachable for any engine states $S_{N-1,j}$, the corresponding $F_{N-1}[j]$ should be set to infinity to rule this engine path out of the future searching range. Also note that, for each $F_{N-1}[j]$, the next engine states to achieve this minimum fuel cost $F_{N-1}[j]$ should be stored to find the optimum engine states path. It is proposed that another storage space is specified, named as $R_i[j]$ to store the next engine states for $F_i[j]$.

Now consider the more general case for any $F_i[j]$ where $i = 1, 2, 3, \dots, N-1$ and $j = 1, 2, 3, \dots M_i$. Recall that the minimum fuel cost engine path through engine state $S_{i,j}$ could be derived from the minimum fuel cost engine path from previously calculated minimum fuel cost $F_{i-1}[j]$ where $j = 1, 2, 3, \dots M_i$. The definition of $F_i[j]$ can be found in (26).

$$F_i[j] = min(F_{i-1}[1]+E_{i,j}, F_{i-1}[2]+E_{i,j}, \dots F_{i-1}[M_{i-1}]+E_{i,j}) \tag{26}$$

By combining (25) and (26), a more general form for the minimum fuel cost $F_i[j]$ is defined.

$$F_i[j] = \begin{cases} E_{N,j} + E_{N-1,1} & \text{if i=N} \\ min(F_{i-1}[1] + E_{i,j}, F_{i-1}[2] + E_{i,j}, & \\ \dots F_{i-1}[M_{i-1}] + E_{i,j}) & \text{if } i \leq N \end{cases} \tag{27}$$

After the final minimum fuel cost $F_1[1]$ is found, it is straightforward to find the next engine states to achieve this fuel cost from the $R_1[1]$. By doing this recursively, each engine state through the whole optimum path can be identified and the minimum fuel cost engine states path is found.

B. Adaptive Online Strategies

Dynamic programming is able to obtain the global optimal engine states path for the journey. However, the whole journey profile must be obtained in advance. This is obviously not possible for online power management [33]. This section will discuss the development of an adaptive online strategy for a potential real time operation using the results generated from DP.

1) Threshold Power Demand: Based on the results of Dynamic Programming, it is found that with a different total power demand, there is a preferred number of engines which produce the best fuel economy, referred to as Preferable Number of Engines (PNE). When the power demand is medium, e.g. during the course of cruising, the global optimization path shows that the best way to supply the traction power is to use only two engines. This type of characteristic can be used to develop a rule for an on-line intelligent power management strategy. From the current power demand, it is possible to calculate the preferable engine power split between the three engines.

Fig.8 illustrates the general idea of preferred engine number decision based on current power demand. The threshold values are decided based on the following two presumptions:

- There are no such engine states with two of the engine output powers being zero for power demand above P_{th1};
- There are no such engine states with any of the engine output powers being zero for power demand above P_{th2}.

These two threshold power values are listed in TABLE III using the results from the DP optimization.

TABLE III
THRESHOLD POWER DEMAND VALUE

Threshold Power Demand	P_{th1}	P_{th2}
Value(kW)	382	686

2) Problem Formulation: After the preferable number of engines based on two thresholds P_{th1} and P_{th2}, has been chosen, each preferable engine output can be determined, as shown in Table IV. $P_{pre}A(N\Delta t)$, $P_{pre}B(N\Delta t)$ and

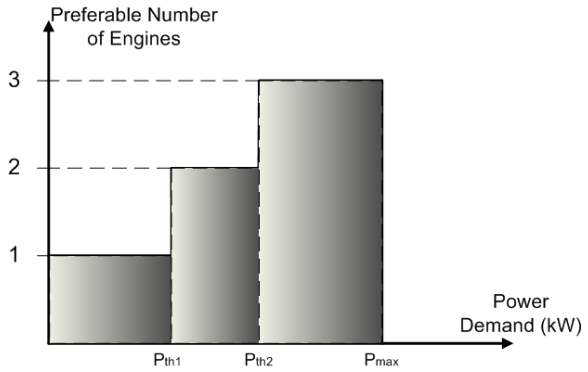

Fig. 8. Preferable number of engine for various power demand

TABLE IV
PREFERABLE POWER DISTRIBUTION BASED ON VARIOUS POWER DEMAND

Power Demand P_d (kW)	Preferable Num. of Engine NoE_{pre}	Preferable Power Distribution
$P_d(N\Delta t) < P_{\text{th1}}(N\Delta t)$	$NoE_{\text{pre}} = 1$	$P_{\text{pre}}A(N\Delta t) = P_d$ $P_{\text{pre}}B(N\Delta t) = 0$ $P_{\text{pre}}C(N\Delta t) = 0$
$P_{\text{th1}}(N\Delta t) < P_d(N\Delta t) \leq P_{\text{th2}}(N\Delta t)$	$NoE_{\text{pre}} = 2$	$P_{\text{pre}}A(N\Delta t) = P_d/2$ $P_{\text{pre}}B(N\Delta t) = P_d/2$ $P_{\text{pre}}C(N\Delta t) = 0$
$P_{\text{th2}}(N\Delta t) < P_d(N\Delta t) \leq P_{\max}$	$NoE_{\text{pre}} = 3$	$P_{\text{pre}}A(N\Delta t) = P_d/2$ $P_{\text{pre}}B(N\Delta t) = P_d/3$ $P_{\text{pre}}C(N\Delta t) = P_d/3$

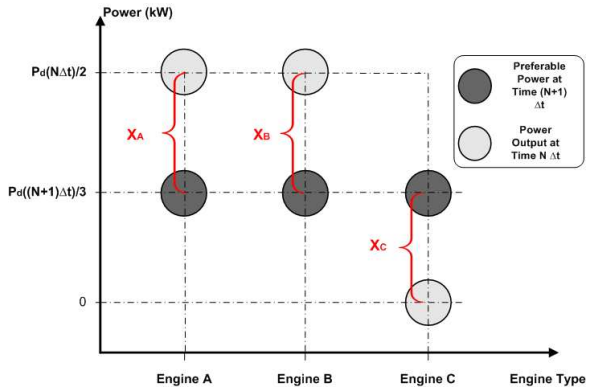

Fig. 9. Illustration for minimization of discrepancy

$P_{pre}C(N\Delta t)$ are the preferable power outputs for each engine. However, there is usually a discrepancy between current engine output and preferable engine output since the power demand changes dynamically. For example, at time $n\Delta t$, the total power requirement is satisfied with two engines working and the preferable engine output equal to the current working engine output. At time $(n+1)\Delta t$, the power demand increases, and engine C is brought into operation. Engine C was giving zero output power at time $n\Delta t$. For engine C, the discrepancy gap between current engine output and current preferable engine output could be very large.

Though it is not possible to achieve the current preferable engine output due to the power slew rate limit, it is possible to minimize the current total discrepancy to achieve an output power as near as the preferable one. Fig. 9 illustrates

TABLE V
ONLINE POWER DISTRIBUTION

$NoE_{\text{opt}} = 1$	$P_A((N+1)\Delta t) = P_d((N+1)\Delta t)$ $P_B((N+1)\Delta t) = 0$ $P_C((N+1)\Delta t) = 0$
$NoE_{\text{opt}} = 2$	$P_A((N+1)\Delta t) = P_A(N\Delta t) + \Delta X_A^*(N\Delta t)$ $P_B((N+1)\Delta t) = P_B(N\Delta t) + \Delta X_B^*(N\Delta t)$ $P_C((N+1)\Delta t) = 0$
$NoE_{\text{opt}} = 3$	$P_A((N+1)\Delta t) = P_A(N\Delta t) + \Delta X_A^*(N\Delta t)$ $P_B((N+1)\Delta t) = P_B(N\Delta t) + \Delta X_B^*(N\Delta t)$ $P_C((N+1)\Delta t) = P_C(N\Delta t) + \Delta X_C^*(N\Delta t)$

the concept of minimization of the discrepancy between the current engine output and next time preferable engine output. At time $N\Delta t$, the power demand is $P_d(N\Delta t)$, the preferable engine number is two. All the engines are working on their preferable states as shown by the grey circles, i.e. $P_A = P_B = P(N\Delta t)/2$ kW and $P_C = 0$ kW. At time $(N+1)\Delta t$, the power demand changes to $P_d((N+1)\Delta t)$ and the preferable number of engines changes to three. At this time step the preferable engine output changes as shown by the black circles in Fig. 9. Each engine output is defined by $P_{pre}A((N+1)\Delta t)$, $P_{pre}B((N+1)\Delta t)$ and $P_{pre}C((N+1)\Delta t)$, and $X_A(N\Delta t)$ $X_B(N\Delta t)$ and $X_C(N\Delta t)$ denotes the discrepancy gap for current engine output and next preferable engine output.

$$X_A(N\Delta t) = P_A(N\Delta t) - P_{pref}A((N+1)\Delta t) \quad (28)$$
$$X_B(N\Delta t) = P_B(N\Delta t) - P_{pref}B((N+1)\Delta t) \quad (29)$$
$$X_C(N\Delta t) = P_C(N\Delta t) - P_{pref}C((N+1)\Delta t) \quad (30)$$

Here we define the total discrepancy gap at time $N\Delta t$ denoted by D_t as follows:

$$D_t(N\Delta t) = |X_A(N\Delta t)| + |X_B(N\Delta t)| + |X_C(N\Delta t)| \quad (31)$$

The optimum change power of each engine, will be the change that minimizes $D_t((N+1)\Delta t)$. $D_t^*((N+1)\Delta t)$ denotes the minimum total discrepancy, $\Delta X_A^*(N\Delta t)$, $\Delta X_B^*(N\Delta t)$, $\Delta X_C^*(N\Delta t)$ to be each change of engine output. One obtains:

$$D_t^*((N+1)\Delta t) = min(D_t((N+1)\Delta t)) \quad (32)$$

A set of variables $\Delta X_A, \Delta X_B, \Delta X_C$ are introduced to minimize $D_t(N\Delta t)$, where $\Delta X_A, \Delta X_B, \Delta X_C$ denotes the change of each engine power output during next time step, shown in (36).

To find the set of engine power change values for the minimum Total Discrepancy, a constrained nonlinear optimisation has been implemented [36]. The paper solves the problem using the Optimization Toolbox$^{\text{TM}}$ in MATLAB. The constraints are listed below:

$$-P_{mps} \leq \Delta X_A(N\Delta t) \leq P_{mps} \quad (33)$$
$$-P_{mps} \leq \Delta X_B(N\Delta t) \leq P_{mps} \quad (34)$$
$$-P_{mps} \leq \Delta X_C(N\Delta t) \leq P_{mps} \quad (35)$$

P_{mps} is the positive Maximum Power Switch in II-B.

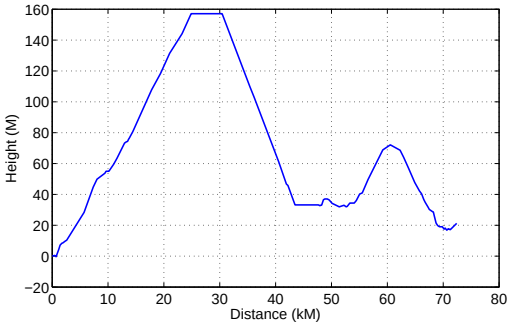

Fig. 10. Altitude profile for the chosen route

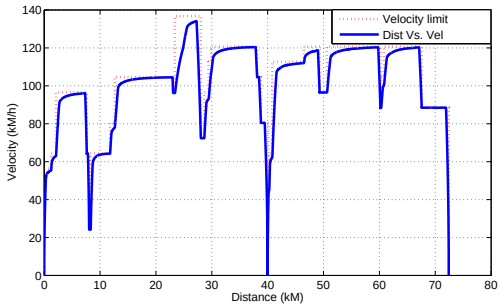

Fig. 11. Velocity profile and velocity limit

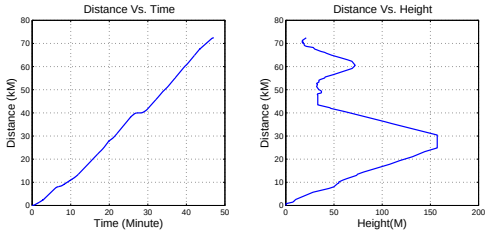

Fig. 12. Distance time graph, and distance height graph

$$\Delta X_A(N\Delta t) + \Delta X_B(N\Delta t) + \Delta X_B(N\Delta t) = P_{diff}(N\Delta t) \tag{36}$$

$P_{diff}(N\Delta t)$ is defined as $P_d((N+1)\Delta t) - P_d(N\Delta t)$ which is the power demand difference between current total engine output and next total engine demand. These constraints are set to ensure the total power demand can be met while the individual engine power changes are minimized. Some points should be noted to avoid undesirable results for practical operations. Some of the notations are listed below:

- NoE_{pre} denotes the current preferable number of engines
- NoE_{act} denotes the number of current working engines
- NoE_{min} denotes the minimum number of working engines for next power demand
- NoE_{opt} denotes the number of engines for optimization, i.e. the minimization process is not always applied for all numbers of engines

TABLE VI
SIMULATION RESULTS COMPARISON

	Energy Consumed (kWh)	Fuel Cost (kg)
Dynamic programming	1888.3	149.1
Rule-based online	1918.4	151.4
Empirical evenly split	2019.8	159.5

$$NoE_{opt} = \begin{cases} \max(NoE_{pre}, NoE_{act}) \\ \text{if } P_{diff}(N\Delta t) < 0 \\ \max(NoE_{pre}, NoE_{act}, NoE_{min}) \\ \text{if } P_{diff}(N\Delta t) \geq 0 \end{cases} \tag{37}$$

The online power distribution is summarized in TABLE V.

C. Results

In Fig. 10, the altitude profile of a typical journey is shown. Fig. 11 illustrates the velocity profile over the route, while showing the velocity limit at various sections of the journey. There is a station at 40 km.

The relationship between the distance and time has been depicted in the left subplot of Fig. 12. The right subplot, for comparative study purposes, is displaying the distance over height so that one could read both graphes to explain the current height at a particular time instance.

The power distribution over the journey time is shown separately in Fig. 13 and incorporatively in Fig. 14. Since the negative braking power demand results in zero power output from each engine, it is emitted in this plot.

Fig. 15 shows that at the beginning of the journey, the power demand is increased from zero to a maximum point to accelerate the vehicle. During this course, each engine starts in sequence. This can be explained by the Preferable Engine Number computation, i.e. the preferable engine number for best fuel economy varies during the initial acceleration phase. The DP helps to locate the power change instant for each engine.

The other three subplots show the power output from engine A, B, and C respectively. Each of the subplots shows results from both the proposed strategies. Fig. 15 shows a magnified view for both strategies. The good level of agreement is due to the intrinsic sub-optimal characteristic. In our rule-based online strategy, the preferable engine output is basically an approximation of the results from DP and not all the approximation can match the global optimization result. Nevertheless, the power distributions using both strategies depict a high degree of agreement. To summarize, realtime operation of power management can benefit from the online strategies developed using off-line global optimization techniques.

TABLE VI shows the simulation results for the three power management strategies. Empirical evenly split strategy means that power requirement is evenly divided between 3 engines all the time. The conversion between the energy consumed and fuel cost is based on the energy density [37]. As listed, the energy density for diesel oil for automotives is 45.6 $\mathrm{GJ/tonne}$.

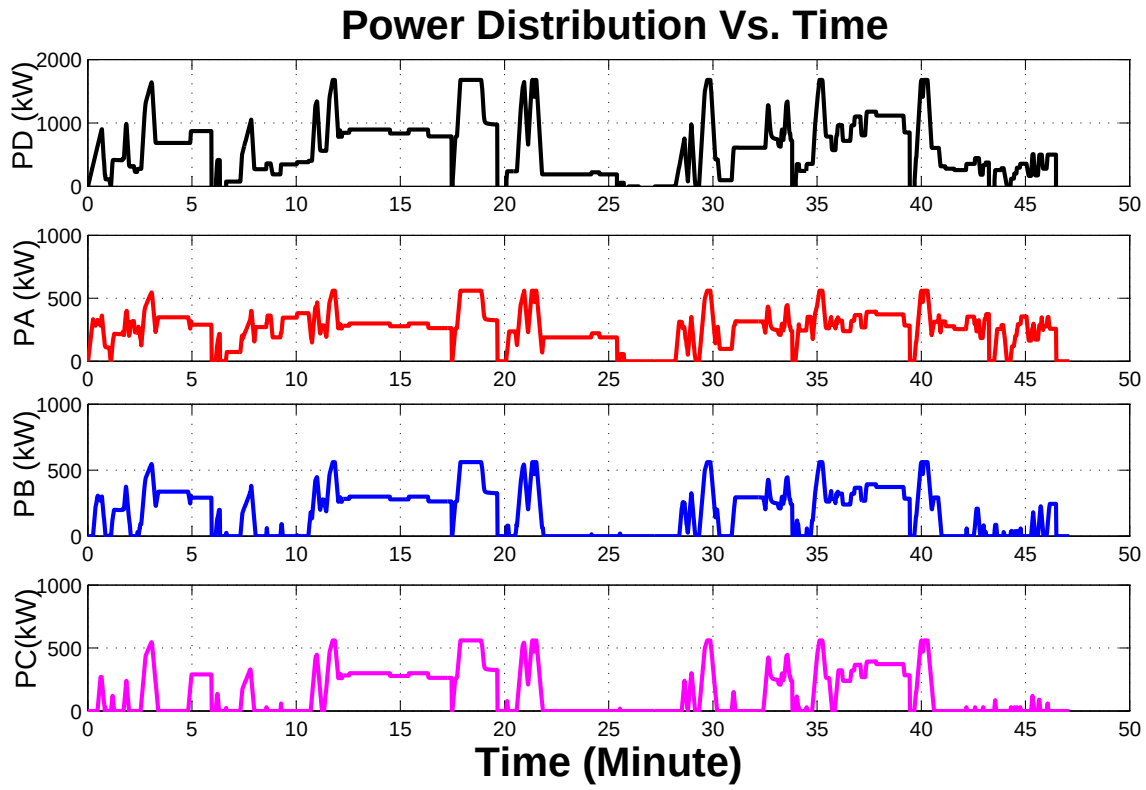

(a) Power distribution over time using dynamic programming

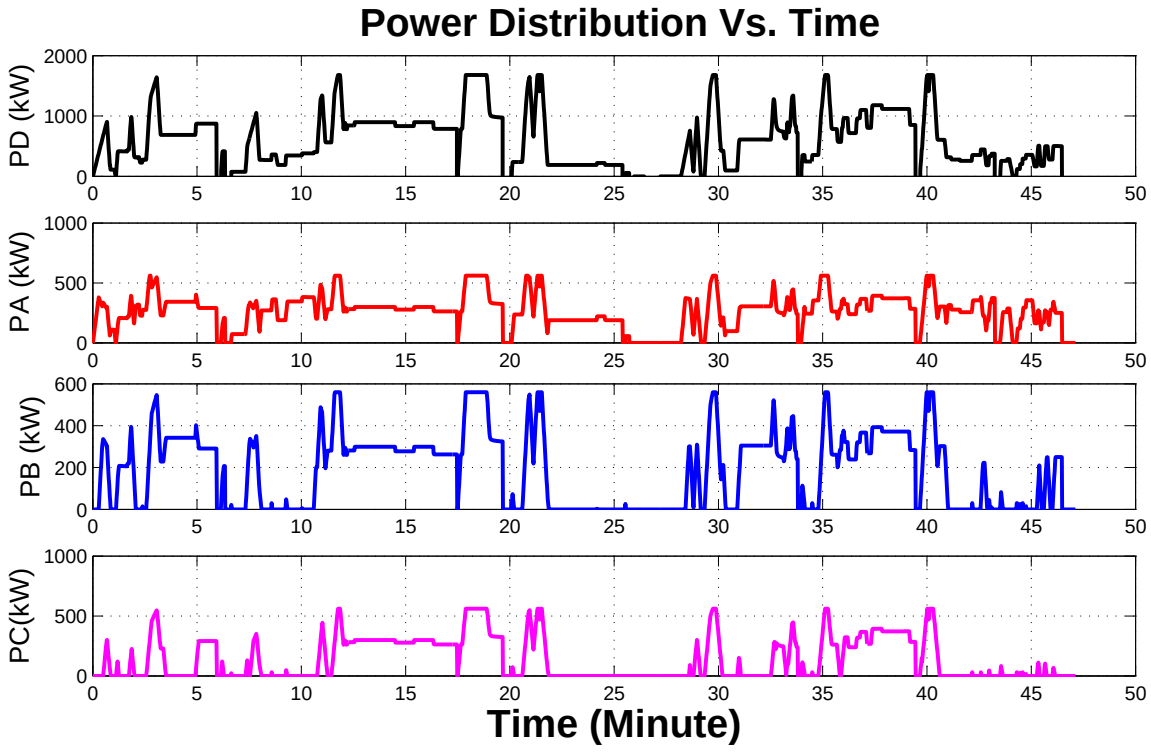

(b) Initial stage of power distribution by online rule based

Fig. 13. Power distribution over time using dynamic programming and online rule based strategy (separate version)

V. Conclusions

Recently, many power management strategies have been applied and realized for hybrid vehicle propulsion system. These strategies are applied to achieve improved fuel economy and better environmental performance. However, so far, these

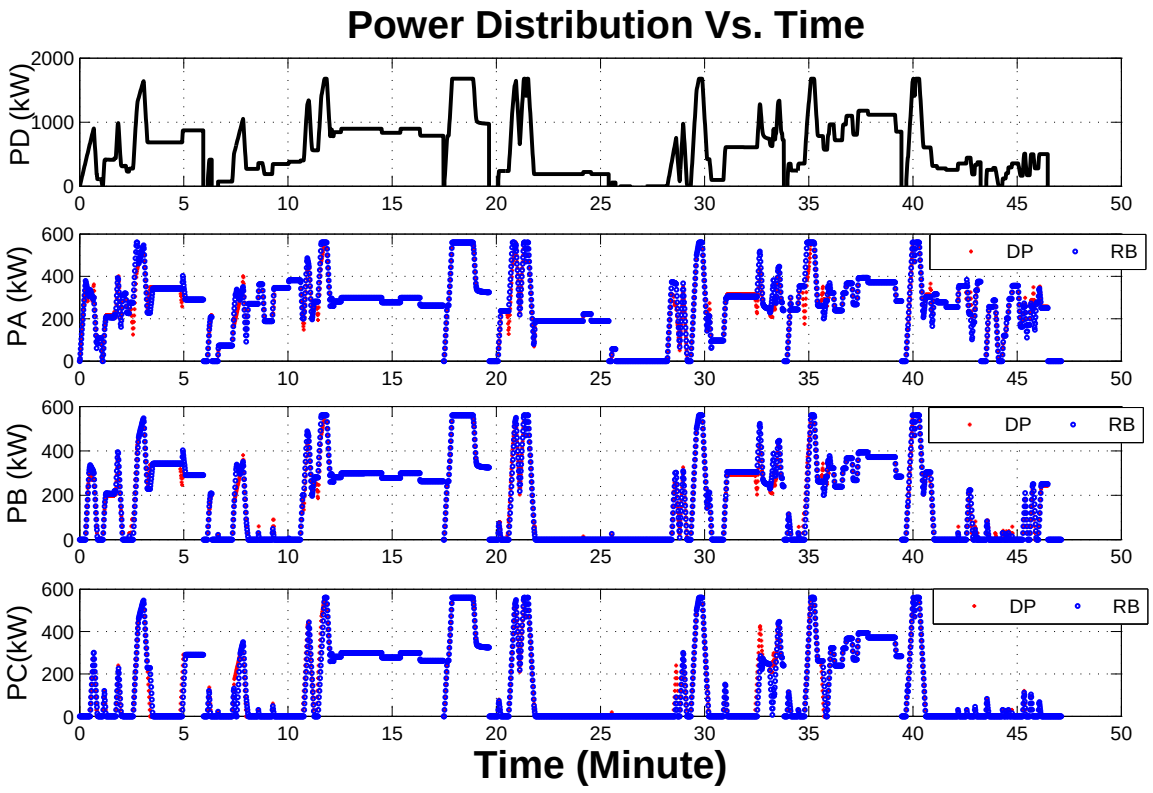

Fig. 14. Power distribution over time using dynamic programming and online rule based strategy (merged version)

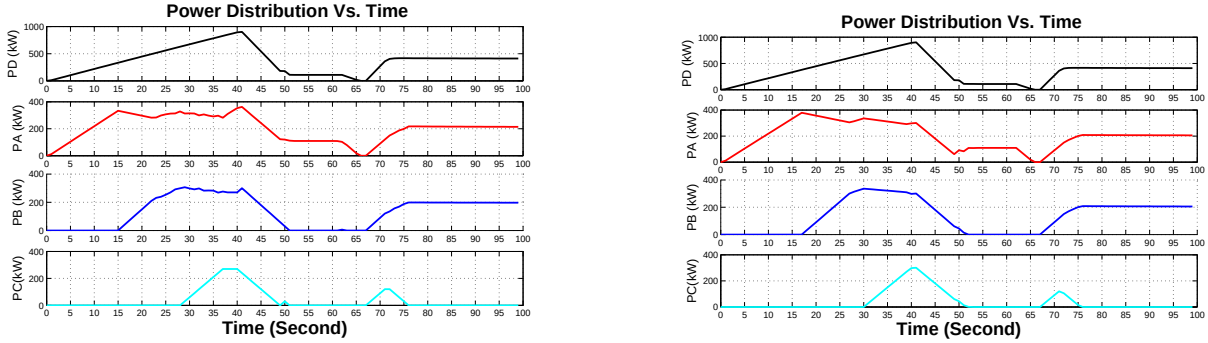

(a) Initial stage of power distribution by DP

(b) Initial stage of power distribution by online rule based

Fig. 15. Initial stage of the power distribution for both power management strategy

technologies have not been considered for a conventional propulsion system. This paper takes a typical British DMU railroad vehicle as a case study and explores the applicability and transferability of an optimal power management strategy. Due to the electrical inter-connection configuration, which enables less engines to work during the lower power requirement journey range, more advanced control strategies are becoming applicable for power management systems.

This paper firstly discussed a platform for the study of the power management strategies: Single Train Motion Simulator (STMS). Through discretization of the basic Newton Equation and modern Resistance Calculation *(Davis Equation)*, a single train motion simulator could be modeled. This simulator is able to take account of the geography and driving style to produce an online output of train position, train velocity, and current power usage etc. Based on this, Dynamic Programming together with an Adaptive on-line rule-based strategy for this typical British DMU train are proposed in this paper. Some improvement and modification has been adopted to decrease the search complexity and thus total computation time while maintaining acceptable optimization precision. Based on the results of dynamic programming, an adaptive online rule-based strategy has also been discussed for further online simulation using large scale non-linear programming.

After transferring the energy consumed into diesel fuel cost, both of the simulation results indicate that a remarkable energy saving has been achieved using both of the two strategies.

This paper considers the engine efficiency map in two

dimensioned space. Further investigation is needed for the study of transient characteristics of the Diesel Engine.

REFERENCES

[1] B. Powell, K. Bailey, and S. Cikanek, "Dynamic modeling and control of hybrid electric vehicle powertrain systems," *Control System Magazine, IEEE*, vol. 18, no. 5, pp. 17–33, 1998.

[2] Anonymous, *Automotive Electronics*, 5th ed. John Wiley Sons Ltd, 2007.

[3] M. Ogasa, "Energy saving and environmental measures in railway techonlogies: Example with hybrid elctric railway vehicles," *IEEJ Transactions on Electrical and Electronic Engineering*, vol. 3, no. 1, pp. 15–20, January 2008.

[4] J. M. Miller, "Power electronics in hybrid electric vehicle applications," in *Conference Proceedings - IEEE Applied Power Electronics Conference and Exposition - APEC*. J-N-J Miller Design Services, P.L.C., 3573 E. Gatzke Road, Cedar, MI 49621, United States: IEEE, 2003, pp. 23–29.

[5] A. D. Napoli, F. Crescimbini, L. Solero, F. Caricchi, and G. F. Capponi, "Multiple-input dc-dc power converter for power-flow management in hybrid vehicles," in *Conference Proceedings - 2002 IEEE Industry Applications Conference 37th IAS Annual Meeting*, IEEE. IEEE, 2002, pp. 1578–1585.

[6] T. Horiba, K. Hironaka, T. Matsumura, T. Kai, M. Koseki, and Y. Muranaka, "Manganese-based lithum batteries for hybrid electric vehicle applications," *Journal of Power Sources*, vol. 119-121, pp. 893–896, 2003.

[7] D. E. Reisner and K. Martin, "Bipolar nickel-metal hydride battery for hybrid vehicles," IEEE. Long Beach, CA, USA: IEEE, May 1994, pp. 111–116.

[8] C. Deng, P.-F. Shi, and S. Zhang, "Development of novel bipolar nickel/metal hydride batteries for hybrid electric vehicles," *Chinese Journal of Chemistry*, vol. 23, no. 2, pp. 221–224, 2005.

[9] D. Ohms, M. Kohlhase, G. Benczur-Urmossy, K. Wiesener, and J. Harmel, "High performance nickel-metal hydride battery in bipolar stack design," *Journal of Power Sources*, vol. 105, no. 2, pp. 120–126, 2002.

[10] K. Chau and Y. Wong, "Overview of power management in hybrid electric vehicles," *Energy Conversion and Management*, vol. 43, no. 15, pp. 1953–1968, 2002.

[11] F. Salmasi, "Control strategies for hybrid electric vehicles: Evolution, classification, comparison, and future trends," *IEEE Transactions on Vehicular Techonolgy*, vol. 56, no. 5, pp. 2390–2404, 2007.

[12] P. Caratozzolo, M. Serra, and J. Riera, "Energy management strategies for hybrid electric vehicles," J.Riera, Ed., IEEE. IEEE International Electric Machines and Drives Conference, 2003, 2003, pp. 241–248.

[13] T. Hofman, M. Steinbuch, R. V. Druten, and A. Serrarens, "Rule-based energy management strategies for hybrid vehicles," *International Journal of Electric and Hybrid Vehicles*, vol. 1, no. 1, pp. 71–94, 2007.

[14] N. A. Kheir, M. A. Salman, and N. J. Schouten, "Emissions and fuel economy trade-off for hybrid vehicles using fuzzy logic," *Mathematics and Computers in Simulation*, vol. 66, no. 2-3, pp. 155–172, 2004.

[15] B. M. Baumann, G. Washington, C. G. Bradley, and G. Rizzoni, "Mechatronic design and control of hybrid electric vehicles," *IEEE/ASME Transaction on Mechatronics*, vol. 5, no. 1, pp. 28–72, 2000, fuzzy logic, load levelling.

[16] H.-D. Lee and S. Seung-Ki, "Fuzzy-logic-based torque control strategy for parallel-type hybrid electric vehicle," *IEEE Transaction on Industrial Electronics*, vol. 45, no. 4, pp. 625–632, 1998.

[17] S. Delprat, T. Guerra, and J. Rimaux, "Optimal control of a parallel powertrain: from global optimization to real time control strategy," vol. 4. Vehicular Technology Conference, IEEE 55th, Fall 2002, pp. 2082–2088.

[18] G. Paganelli, S. Delprat, T. Guerra, J. Rimaux, and J. Santin, "Equivalent consumption minimization strategy for parallel hybrid powertrains," vol. 4. Vehicular Technology Conference IEEE 55th, Spring 2002, pp. 2076–2081.

[19] T. Ogawa, H. Yoshihara, S. Wakao, K. Kondo, and M. Kondo, "Energy consumption analysis of fc-edlc hybrid railway vehicle by dynamic programming." 2007 European Conference on Power Electronics and Applications, 2007.

[20] ——, "Design estimation of the hybrid power source railway vehicle based on the multiobjective optimization by the dynamic programming," *IEEJ Transactions on Electrical and Electronic Engineering*, vol. 3, no. 1, pp. 48–55, 2008.

[21] E. D. Tate and S. P. Boyd, "Finding ultimate limits of performance for hybrid electric vehicles," vol. 109, SAE Future Transportation Technology Conference and Exposition. SAE International, Warrendale, Pennsylvania, USA, August 2000.

[22] B. Huang, X. Shi, and Y. Xu, "Parameter optimization of power control strategy for series hybrid electric vehicle," Evolutionary Computation, 2006. CEC 2006. IEEE Congress on. IEEE, pp. 1989–1994.

[23] M.-G. Morteza and A. Poursamad, "Application of genetic algorithm for simultaneous optimisation of hev component sizing and control strategy," *International Journal of Alternative Propulsion*, vol. 1, no. 1, pp. 63–78, 2006.

[24] A. Sciarretta, M. Back, and L. Guzzella, "Optimal control of parallel hybrid electric vehicles," *IEEE Transactions on Control Systems Technology*, vol. 12, no. 3, pp. 352–363, 2004.

[25] S. Delprat, T. M. Guerra, and J. Rimaux, "Control strategies for hybrid vehicles: optimal control," vol. 3. Vehicular Technology Conference, IEEE 56th, Fall 2002, pp. 1681–1685.

[26] Siemens, "Disiro uk dmu class 185," Siemens Transportation, Technique Report, 2004, www.siemenstransportation.co.uk/pdfs/185.pdf.

[27] N. Donovan, "Trans-pennine trains get greener," *Railway Gazette International*, vol. 164, no. 9, p. 715, Sept 2008.

[28] R. Hill, "Electric railway traction. part 1: Electric traction and dc traction motor drives," *Power Engineering Journal*, vol. 8, no. 1, pp. 47–56, 1994.

[29] B. P. Rochard and F. Schmid, "A review of methods to measure and calculate train resistances," *Proceedings of the Institution of Mechanical Engineers, Part F: Journal of Rail and Rapid Transit*, vol. 214, no. 4, pp. 185–199, 2000.

[30] T. Hofman, M. Steinbuch, R. V. Druten, and A. Serrarens, "Rule-based energy management strategies for hybrid vehicles," *International Journal of Electric and Hybrid Vehicles*, vol. 1, no. 1, pp. 71–94, 2007.

[31] S. Hillmansen and C. Roberts, "Energy storage devices in hybrid railway vehicles: A kinematic analysis," *Proceedings of the Institution of Mechanical Engineers, Part F: Journal of Rail and Rapid Transit*, vol. 221, no. 1, pp. 135–143, 2007.

[32] R. E. Bellman, *Dynamic programming*, ser. Rand Corporation research study. Princeton : Princeton University Press, 1957.

[33] Y. Zhu, Y. Chen, G. Tian, H. Wu, and Q. Chen, "A four-step method to design an energy management strategy for hybrid vehicles." 2004 American Control Conference, June 2004.

[34] A. Lew and H. Mauch, *Dynamic programming: A Computational Tool*, ser. Studies in Computational Intelligence. Berlin: Spring, 2007, vol. 38.

[35] T. H. Corman, C. E. Leiserson, R. L. Rivest, and C. Stein, *Introduction to Algorithms*, 2nd ed. The MIT Press, Sep 2001.

[36] R. H. Byrd, M. E. Hribar, and J. Nocedal, "An interior point algorithm for large scale nonlinear programming," *SIAM Journal on Optimization*, vol. 9, no. 4, pp. 877–900, 1997.

[37] IOR, "Fuel energy density," http://www.ior.com.au/ecflist.html, accessed at June 3rd 2009.

PLACE PHOTO HERE

Shaofeng Lu Biography to follow.

Stuart Hillmansen Biography to follow.

Clive Roberts Biography to follow.